HHS Public Access

Author manuscript

Curr Biol. Author manuscript; available in PMC 2018 August 21.

Published in final edited form as:

Curr Biol. 2017 August 21; 27(16): 2465–2475.e3. doi:10.1016/j.cub.2017.06.084.

Direct midbrain dopamine input to the suprachiasmatic nucleus accelerates circadian entrainment

Ryan M. Grippo[1], **Aarti M. Purohit**[1], **Qi Zhang**[1], **Larry S. Zweifel**[2], and **Ali D. Güler**[1,3,4]

[1]Department of Biology, University of Virginia, 485 McCormick Road Charlottesville, Virginia 22904, USA

[2]Departments of Pharmacology and Psychiatry & Behavioral Sciences, University of Washington, 1959 NE Pacific Street Seattle, Washington 98195, USA

[3]Department of Neuroscience, School of Medicine, University of Virginia, 409 Lane Road Charlottesville, Virginia 22908, USA

Summary

Dopamine (DA) neurotransmission controls behaviors important for survival including voluntary movement, reward processing, and detection of salient events such as food or mate availability. Dopaminergic tone also influences circadian physiology and behavior. Although the evolutionary significance of this input is appreciated, its precise neurophysiological architecture remains unknown. Here, we identify a novel, direct connection between the DA-neurons of the ventral tegmental area (VTA) and the suprachiasmatic nucleus (SCN). We demonstrate that D1 dopamine receptor (Drd1) signaling within the SCN is necessary for properly timed resynchronization of activity rhythms to phase-shifted light:dark cycles and that elevation of DA tone through selective activation of VTA DA-neurons accelerates photoentrainment. Our findings demonstrate a previously unappreciated role for direct DA input to the master circadian clock and highlight the importance of an evolutionarily significant relationship between the circadian system and the neuromodulatory circuits that govern motivational behaviors.

In Brief

Grippo et al. demonstrate a direct functional connection from the midbrain dopamine neurons to the central circadian clock. This D1 dopamine receptor dependent connection regulates the rate of entrainment, highlighting the critical role for dopamine signaling in the modulation of central circadian rhythms.

Correspondence: aguler@virginia.edu (A.D.G).

[4]Lead contact

Author Contributions

R.M.G and A.D.G conceived and designed the experiments. R.M.G, A.M.P, and Q.Z performed experiments. R.M.G, A.M.P, Q.Z, and A.D.G analyzed the data. L.S.Z provided re-expression viral constructs and expertise. A.D.G supervised the research. R.M.G and A.D.G wrote the manuscript with input from coauthors.

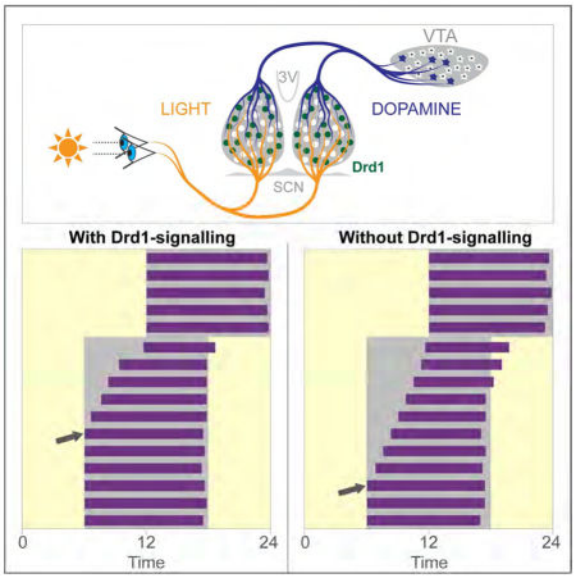

Keywords

Hypothalamic circuitry; SCN; circadian entrainment; photoentrainment; opamine; D1 dopamine receptor

Introduction

Circadian rhythms have evolved to synchronize (entrain) physiological processes to predictable environmental events, such as sunrise and sunset. This ensures that coordinated biological responses occur within a temporal niche. In mammals, circadian rhythms are driven by the suprachiasmatic nucleus (SCN), which controls downstream daily oscillatory processes including the sleep-wake cycle, body temperature fluctuation, hormone production, and feeding behavior [1, 2]. The short-term desynchrony between the astronomical day and endogenous circadian rhythms that is experienced by humans during shift work or transmeridian travel (jet-lag) leads to general malaise, insomnia, and cognitive deficiencies [3]. When prolonged, such misalignment results in higher incidences of obesity, cardiovascular disease, cancer, and even increased mortality [4, 5]. Light detected by the retina is the main driver synchronizing the phase of endogenous oscillations to external circadian cycles, a process termed photoentrainment [6–8]. In addition, non-photic environmental signals including restricted food access, exercise, and salient cues such as fear-inducing events, also affect circadian entrainment [9]. Although the neuronal circuitry governing photoentrainment is well characterized [7, 10], how non-photic information integrates with this system to create a comprehensive circadian response is poorly understood.

Dopamine (DA) has been implicated in various behaviors that show periodicity, such as locomotion, reward seeking behavior, and wakefulness [11]. Prior to the development of the retinohypothalamic tract, DA is thought to act as a non-photic entrainment cue in the embryonic and early postnatal SCN, synchronizing the circadian rhythm of the mother and

her offspring [12, 13]. Since pharmacological stimulation of the DA system in adult rodents and primates fails to elicit behavioral responses or induce c-Fos expression within the SCN, it has been assumed that the SCN loses sensitivity to DA shortly after birth [12, 14]. Nevertheless, dopaminergic agents, such as methamphetamine or cocaine, have been shown to influence entrainment to the light:dark (LD) cycle in adult animals [11]. While it remains unclear whether SCN-dependent photoentrainment is directly influenced by the dopaminergic system, DA signaling in the dorsal striatum has been proposed to regulate non-photic entrainment to timed food availability [15], an SCN-independent behavior [16, 17].

In this study, we challenge the consensus that SCN responsiveness to DA is lost during development, and provide evidence that dopaminergic signaling within the SCN continues to influence circadian photoentrainment through adulthood. First, we demonstrate that selective activation of D1 dopamine receptor (Drd1) expressing SCN (Drd1-SCN) neurons shifts the phase of circadian rhythms, mimicking the phase-shifting response to light. Second, we show that *Drd1a*-null (Drd1-KO) mice exhibit a slow rate of photoentrainment in response to a phase shift in the light cycle, which is rescued by re-expression of Drd1 exclusively within the SCN. Third, we identify a direct neuronal connection from DA-neurons of the ventral tegmental area (VTA) to the central pacemaker, and lastly, we report that specific activation of this midbrain DA-neuron population accelerates entrainment to a light cycle shift. We conclude that Drd1-dependent DA-signaling within the SCN modulates the rate of synchronization of circadian rhythms to changes in the environmental conditions.

Results

Drd1 is Expressed in the SCN Through Adulthood

The presence of dopamine receptor *Drd1a* mRNA is well documented within the SCN of adult rodents, non-human primates, and humans; however, its functional role remains inconclusive [12, 14, 18]. In line with reported expression profiles for *Drd1a*, we observed Drd1 immunoreactivity in the SCN of wild-type mice but not in *Drd1a* knockout (Drd1-KO) animals in which both *Drd1a* alleles were replaced by the Cre recombinase open reading frame (Cre; Figure 1A) [19]. We confirmed functional Cre expression in the SCN of heterozygous Drd1-Cre mice by crossing them to ROSA26-tdTomato animals (Ai14) that Cre-dependently express tdTomato red fluorescent protein, and we observed signal throughout the SCN (Figures 1B and 1C, Figure S1) [20]. As this could be attributable to developmental expression, we validated adulthood *Drd1a* promoter driven Cre expression through bilateral infusion of a Cre-dependent mCherry reporter adeno associated virus (AAV), AAV-DIO-mCherry, to the SCN of 8 week old Drd1-Cre mice and observed mCherry signal within a subset of SCN neurons (Figures 1D and 1E).

Activation of Drd1-SCN Neurons Induces Phase Shift of Behavioral Rhythms

The SCN is comprised of a heterogeneous population of cells that differ in their oscillatory activities, neurotransmitters, and responses to light [21–24]. Individual cellular oscillators couple to produce a stable, coherent, rhythmic output; however, not all SCN neurons contribute equally to the production and modulation of circadian rhythms [25]. To determine

whether Drd1-SCN neurons influence the phase of the endogenous clock, we sought to activate this population using Cre-conditional chemogenetic methods under constant conditions and monitor the effect on wheel running activity rhythms. To this end, we bilaterally delivered a Cre-dependent AAV encoding either hM3Dq- mCherry (hM3Dq), a G_q-coupled designer receptor exclusively activated by a designer drug (DREADD; AAV-DIO-hM3Dq), or mCherry (AAV-DIO-mCherry) as a control, to the SCN of Drd1-Cre mice. After stable entrainment of wheel running activity, we introduced both groups to constant darkness (DD) [26, 27]. Viral treatment alone had no effect on the phase angle of entrainment during the 12-hour:12-hour light:dark (LD) cycle or the length of free-running period in DD (Table S1). We then evaluated the behavioral response to selective activation of Drd1-SCN neurons in free running animals at three circadian time points (Figures 2A–2C). Administration of the DREADD-specific agonist, clozapine-N-oxide (CNO; 1 mg/kg, i.p.) six hours prior to activity onset at circadian time (CT) 6 did not produce a significant phase shift in either group (control: −9.00 ± 3.18 minutes; hM3Dq: −14.70 ± 9.71 minutes; p = 0.633, Student's two tailed t-test; n = 6–8/group; Figures 2A and 2D). However, CNO administration two hours after activity onset at CT 14 induced a significantly larger phase delay of wheel running activity in hM3Dq mice compared to mCherry controls (control: −7.33 ± 4.54 minutes; hM3Dq: −51.63 ± 28.18 minutes; p = 0.0009, Student's two tailed t-test; n = 7–9/group; Figures 2B and 2D). Additionally, CNO administration ten hours after activity onset at CT 22 resulted in a significantly larger phase advance (controls: 0.46 ± 4.08 minutes; hM3Dq: 44.22 ± 8.80 minutes; p = 0.0007, Student's two tailed test; n = 8–10/group; Figures 2C and 2D). The responsiveness of hM3Dq-expressing Drd1-SCN neurons to CNO administration was verified by quantification of SCN c-Fos induction two hours after lights-off at *Zeitgeber* time (ZT) 14 (Figure 2E). We observed a robust increase in c-Fos expression within the SCN of hM3Dq mice compared to mCherry controls (control: 32.10 ± 7.00 c-Fos positive cells/mm^2; hM3Dq: 630.30 ± 117.20 c-Fos positive cells/mm^2; p = 0.0005, Student's two tailed t-test; n = 7–9/group; 5 SCN sections/mouse). The magnitude of behavioral phase delays at CT 14 correlated positively with the amount of c-Fos induced within the SCN (R^2 = 0.8844, p < 0.0001; Figure 2F). These findings demonstrate that Drd1-SCN neuron activation mimics the effects of light pulses during the early and late subjective night, and fails to elicit a response during the mid-subjective day when the circadian clock is sensitive to non-photic entrainment cues [28, 29].

Drd1-KO Mice Exhibit a Slow Rate of Photoentrainment

Since Drd1-SCN neuron activation resembles the phase response to photic cues, we sought to determine if Drd1-dependent signaling is an essential component of photoentrainment. Comparison of circadian wheel-running activities between wild-type and Drd1-KO mice revealed no significant differences in several circadian parameters including phase angle of entrainment in a LD cycle or free running period length in DD (Table S1). An acute light pulse (15 minutes, 100 μW/cm^2) presented at CT 14 or CT 22 also produced similar phase delays or advances, respectively (CT 14; wild-type: −114.20 ± 5.09 minutes, Drd1-KO: −126.70± 8.02 minutes; p = 0.19, Student's two tailed t-test, n = 6–9/group; CT 22; wild-type: 45.75 ± 3.91 minutes, Drd1-KO: 55.30 ± 5.20 minutes; p = 0.16, Student's two tailed t-test; n = 6–8/group, Figures S2A–S2C). Additionally, negative masking behavior in response to a 3-hour light pulse during the active period was normal in Drd1-KO mice,

exhibiting significant suppression of wheel running activity that was comparable to wild-type controls (wild-type: 96 ± 2.67%; Drd1-KO: 92 ± 1.60%; p = 0.28, Student's two tailed t-test; n = 8/group; Figure S2D and S2E). Despite these similarities in light-dependent behavioral responses, when challenged by a 6-hour advance in the LD cycle, simulating transmeridian travel, Drd1-KO mice took significantly longer to entrain activity rhythms (wild-type: 6.65 ± 0.28 days; Drd1-KO: 8.58 ± 0.28 days; p < 0.0001, Student's two tailed t-test; n = 26/group; Figures 3A–3C). Analysis of daily cumulative phase shifts revealed no differences on day 1 of the LD shift, when the time of 'lights-off' was advanced six hours (Figure 3D). However, on day 2, after the introduction of the new light phase, wild-type animals advanced their activity onset significantly more than Drd1-KO mice (cumulative phase shift on day 2; wild-type: 134.0 ± 19.06 minutes; Drd1-KO: 50.6 ± 7.29 minutes; p < 0.0001, repeated-measures two-way ANOVA with Bonferroni *post hoc* comparison; n = 26/group; Figure 3D). As a result, Drd1-KO mice had a marked reduction in the rate of entrainment (minutes/day) during the initial stage of synchronization compared to wild-type controls (days 0–4; wild-type: 70.77 ± 0.09 minutes/day; Drd1-KO: 41.76 ± 3.55 minutes/day; p < 0.0001, repeated-measures two-way ANOVA with Bonferroni *post hoc* comparison; n = 26/group; Figure 3E). When the LD cycle was delayed six hours, Drd1-KO mice exhibited similar deficits in photoentrainment duration (wild-type: 5.75 ± 0.25 days; Drd1-KO: 7.67 ± 0.36 days; p = 0.0002, Student's two tailed t-test; n = 12/group; Figures S3A and S3B) and rate (days 0–4; wild-type: 87.6 ± 5.99 minutes/day; Drd1-KO: 55.42 ± 3.27 minutes/day; p < 0.0001, repeated-measures two-way ANOVA with Bonferroni *post hoc* comparison; n = 12/group; Figure S3C). The delayed rate of resynchronization observed in Drd1-KO mice following advancing or delaying shifts demonstrates that Drd1 signaling is required for efficient re-entrainment.

Drd1 Modulation of Entrainment Rate Requires Light Input

To test whether the influence of Drd1 signaling during circadian re-entrainment requires photic input, we advanced the time of lights-off by six hours and immediately placed wild-type and Drd1-KO mice into constant darkness (Figure 4A). Interestingly, no significant differences in phase shift duration were observed between genotypes on either day 1 or day 2 following the LD cycle shift (cumulative phase shift on day 2; wild-type: 42.53 ± 6.46 minutes; Drd1-KO: 36.38 ± 5.75 minutes; p = 0.9326, repeated-measures two-way ANOVA with Bonferroni *post hoc* comparison; n = 8/group; Figure 4B). However, in line with results observed during the complete 6-hour LD shift (Figures 3B and 3D), wild-type animals exposed to a six hour advance in the dark phase, followed by a 12-hour cycle of light exposure prior to placement into DD (Figure 4C), experienced a robust shift in activity onset on day 2 compared to Drd1-KO mice (cumulative phase shift on day 2; wild-type: 110.80 ± 16.95 minutes; Drd1-KO: 52.18 ± 9.76 minutes; p = 0.0011, repeated-measures two-way ANOVA with Bonferroni *post hoc* comparison; n = 8/group; Figure 4D). Thus, Drd1 signaling may be regulating the photoentrainment rate by modulating the sensitivity of the circadian system to canonical photic inputs.

Re-expression of Drd1 within the SCN of Drd1-KO Mice is Sufficient to Rescue Entrainment Rate Deficit

As Drd1 is expressed throughout the brain and peripheral organs [30], we sought to determine whether its absence specifically within the central oscillator was responsible for the delayed entrainment rate observed in Drd1-KO mice (Figures 3 and 4). To test the role of SCN-Drd1 signaling during photoentrainment, we restored Drd1 expression within the SCN of Drd1-KO mice and assessed their ability to entrain to a light cycle shift. We accomplished SCN-specific rescue of Drd1 expression by delivering an AAV containing a Cre-dependent Drd1-HA transgene (AAV-DIO-Drd1-HA) to the SCN of homozygous Drd1-Cre knock-in mice (Drd1-KO-Rescue; Figure 5A) [31]. Drd1-KO mice that received AAV-DIO-mCherry or a Cre-dependent AAV encoding the light activated, membrane localized cation channel Channelrhodopsin-2 (AAV-DIO-ChR2-eYFP) were used as controls. Successful introduction of AAV-DIO-Drd1-HA was determined by immunohistochemistry (Figure 5B). In response to a 6-hour advance in the LD cycle, restoration of Drd1 within the SCN completely rescued the rate of circadian photoentrainment in Drd1-KO mice to wild-type levels. No significant differences were observed between mCherry or ChR2 groups, however, both controls took significantly longer to entrain than Drd1-KO-Rescue mice (Drd1-KO-Rescue: 6.31 ± 0.26 days; ChR2: 7.88 ± 0.40 days, $p = 0.0085$; mCherry: 7.92 ± 0.34 days, $p = 0.0023$; one-way ANOVA with Bonferroni *post hoc* analysis; n = 8–13/group; Figures 5C–5E). The most prominent difference once again occurred two days after the shift following the first ‘lights-on’ segment of the new LD cycle (cumulative phase shift on day 2: Drd1-KO-Rescue: 138.30 ± 31.22 minutes; ChR2: 58.28 ± 11.00 minutes, $p = 0.0117$; mCherry: 70.26 ± 7.82 minutes, $p = 0.0181$; repeated-measures two-way ANOVA with Bonferroni *post hoc* comparison; n = 8–13/group; Figure 5F). Like wild-type mice, only virally restored mice displayed a normal rate of entrainment during the initial phase of the LD shift (days 0–4; Drd1-KO-Rescue: 73.80 ± 6.87 minutes/day; ChR2: 47.9 ± 4.09 minutes/day; $p = 0.0024$; mCherry: 51.28 ± 3.66 minutes/day, $p = 0.0003$; repeated-measures two-way ANOVA with Bonferroni *post hoc* comparison; n = 8–13/group; Figure 5G). When the LD cycle was delayed six hours, Drd1-KO-Rescue mice also exhibited a standard duration of photoentrainment (ChR2: 5.17 ± 0.40 days; Drd1-KO: 7.50 ± 0.27 days; $p = 0.0003$, Student’s two tailed t-test; n = 6–8/group; Figures S3D and S3E) and rate (days 0–4; wild-type: 94.45 ± 4.72 minutes/day; Drd1-KO: 59.97 ± 3.32 minutes/day; $p < 0.0001$, repeated-measures two-way ANOVA with Bonferroni *post hoc* comparison; n = 6–8/group; Figure S3F). These rescue studies demonstrate that delayed photoentrainment in Drd1-KO mice is caused primarily by the absence of Drd1 signaling within the SCN.

The SCN Receives VTA DA-neuron Innervation

After establishing a significant role for Drd1 expression in governing the rate of circadian photoentrainment within the adult mammalian SCN, we aimed to determine the potential source of dopaminergic input to the central clock. The existence of dopaminergic axonal fibers within the SCN and peri-SCN previously has been identified in hamsters, rats, and mice [32–34]. Consistent with previously published levels in other mammals, we detected 3.79 ± 1.20 pg/mm^3 of DA in the SCN of wild-type mice (n = 5 mice) using high performance liquid chromatography (distinguished from other monoamines and DA metabolites by its specific retention time) [35]. To demonstrate the presence of synaptic

release machinery in DA-neurons within the SCN, we crossed mice expressing Cre under the control of the DA transporter promoter (DAT-Cre) with ROSA26-Flox-synaptophysin-tdTomato (Ai34D) mice, which facilitated the expression of tdTomato specifically in synaptic terminals of dopaminergic neurons (Figure 6A) [36]. We observed tdTomato positive structures within the nucleus accumbens (NAc), a well-known projection site of DA-neuron populations, and the SCN of these mice (Figures 6B and 6C). To screen for potential DA-neuron populations providing this input, we delivered retrogradely transported red fluorescent beads (retrobeads) to the SCN of wild-type mice (Figure 6D and 6E). Three weeks after surgery, we examined the brains of injected mice for retrobeads within the major DA-neuron populations. Colocalization of retrobeads with tyrosine hydroxylase (TH), the rate-limiting enzyme in DA synthesis, was consistently observed within the ventral tegmental area (VTA; Figure 6F). Although we cannot definitively rule out dopaminergic projections from other regions, we did not observe colocalization in the olfactory bulb, zona incerta, substantia nigra, or the retrorubral field (n = 6 mice; Figure S4a). When retrobeads were delivered dorsal to the SCN, no colocalization was observed (n = 12 mice). To determine the efficiency of retrobead uptake by the VTA DA-neurons, we targeted the NAc with retrobeads and observed that a larger portion of DA-neurons project to the NAc relative to the SCN (Figure S4). Next, we sought to confirm direct VTA-DA neuron innervation of the SCN by injecting AAV-DIO-mCherry into the VTA of adult DAT-Cre mice (Figure 6G). We observed dense mCherry positive fiber innervation within the NAc (Figure 6H), and additionally, within and immediately surrounding the SCN (n = 4 mice; two weeks post-injection; Figure 6I). Together, these results demonstrate the existence of a VTA DA-neuron population that directly innervates the SCN.

Activation of VTA DA-neurons Accelerates Rate of Entrainment

DA-neurons of the VTA are regulators of motivational processes and have recently been implicated in ethologically relevant sleep related behaviors [37, 38]. To examine whether increased activity of VTA DA-neurons influences the rate of circadian photoentrainment, we delivered AAV-DIO-hM3Dq or AAV-DIO-mCherry to the VTA of DAT-Cre mice (Figure 7A) [39–41]. Immunohistochemical analysis revealed that 93.25 ± 2.65% of mCherry expressing cells co-localized with TH positive neurons in the VTA (Figure 7A, n = 3 mice; 4 VTA sections/mouse). Additionally, administration of CNO at ZT 14 (1 mg/kg; i.p.) resulted in significantly greater c-Fos induction within the VTA of hM3Dq mice compared to mCherry controls (control: 56.53 ± 6.12 c-Fos positive cells/mm^2; hM3Dq: 940.16 ± 74.27 c-Fos positive cells/mm^2; p = 0.0067, Student's two tailed t-test; n = 3/group; 4 VTA sections/mouse; Figures 7B and 7C, Figures S5A and S5B). Viral treatment produced no effect on free-running period or the phase angle of entrainment (Table S1). However, following CNO administration immediately prior to a 6-hour advance in the LD cycle, hM3Dq mice entrained significantly faster than mCherry controls (control: 7.50 ± 0.42 days; hM3Dq: 5.78 ± 0.22 days; p = 0.0020, Student's two tailed t-test; n = 8–9/group; Figures 7D–7F). Interestingly, in line with the entrainment differences between wild-type and Drd1-KO mice, the most prominent advance occurred on the second day of the LD cycle shift after DA-neuron stimulation (cumulative phase shift duration on day 2; control: 65.40 ± 10.10 minutes; hM3Dq: 158.1 ± 32.14 minutes; p = 0.0197, repeated-measures two-way ANOVA with Bonferroni *post hoc* comparison; n = 8–9/group; Figure 7G). Consequently, hM3Dq

mice exhibited an accelerated rate of entrainment within the initial period of the light cycle shift (days 0–4; control: 51.91 ± 5.39 minutes/day; hM3Dq: 72.92 ± 7.07 minutes/day; p = 0.0156, repeated-measures two-way ANOVA with Bonferroni *post hoc* comparison; n = 8–9/group; Figure 7H). To confirm the necessity of photic input following the elevation in the DA tone for this response, we administered CNO or saline to hM3Dq mice prior to a 6-hour advance of the LD cycle and immediately placed them into DD (Figure S5C). No significant difference was observed in the duration of shift between saline or CNO injected hM3Dq mice on either day of analysis (cumulative phase shift duration on day 2; saline: 60.38 ± 8.74 minutes; CNO: 56.32 ± 9.97 minutes; p = 0.9847, repeated-measures two-way ANOVA with Bonferroni *post hoc* comparison; n = 8/group; Figure S5D), demonstrating that elevated DA tone by itself is not sufficient to phase-shift the circadian clock. Rather, these findings demonstrate that the selective activation of VTA DA-neurons increases the responsiveness of the circadian clock to photic inputs, allowing for efficient photoentrainment.

Discussion

The circadian system has evolved to predict and adjust to daily changes in environmental conditions. For humans, the advent of artificial lighting has introduced conditions that exceed the ability of our circadian axis to swiftly synchronize to constantly changing environmental, social, and economic pressures. Here, we show that the SCN receives direct input from VTA DA-neurons (Figure 6) consistent with previous findings demonstrating that electrolytic lesion of midbrain dopaminergic neurons leads to a 40% reduction of DA levels within the SCN [42]. Most notably, we demonstrate that stimulation of VTA DA-neurons accelerates entrainment to a shift in the light cycle, especially within the initial first two days of this response (Figure 7). In addition, we observed that the continuation of a shifted LD cycle is necessary for the potentiation of the phase shifts in response to elevated DA tone (Figure S5C and S5D), suggesting that DA signaling enhances photic resetting.

Extensive work has been conducted to discover a variety of DA neurotransmission-associated pacemakers such as the food entrainable oscillator, the dopamine ultradian oscillator, and the methamphetamine-sensitive circadian oscillator [16, 41, 43–45]. Intriguingly, these oscillators have all been found to drive cyclic rhythms in the absence of a functional SCN. However, when the central circadian pacemaker is intact, proper integration with these extra-SCN oscillators is necessary for a comprehensive biological timing process. The persistent expression of Drd1 within the adult SCN suggests the existence of Drd1-dependent dopaminergic modulation of central circadian rhythms. In addition to our findings (Figure 2), two other reports have used Drd1-mediated intersectional genetics to show that, first, altering firing rate in Drd1-SCN neurons entrained behavioral rhythms to the time of optogenetic stimulation [46] and second, Drd1-SCN neurons were the rate determining cells within the SCN circuit in a temporally chimeric mouse model [47]. Here, we demonstrate that selective activation of Drd1 neurons within the SCN phase shifts behavioral rhythms when the circadian system is most sensitive to light, thereby proposing a functional role for endogenous Drd1 signaling within the central clock in the modulation of photoentrainment.

Previous studies have shown that DA, Drd1, and Drd2 signaling within the retina and striatum influences circadian clock gene expression, light adapted vision, and circadian wheel-running patterns [48–51]. Our experiments demonstrate that Drd1 expression within the SCN influences the rate of circadian entrainment to a shifted light cycle. In support of this claim, loss of Drd1 leads to a significantly reduced rate of photoentrainment, which is rescued by re-expression of Drd1 within the SCN (Figures 5 and 6), even though the absence of Drd1 has a moderate increase in locomotor activity [19, 52] and does not affect most circadian parameters (Figure S2 and Table S1). Thus, we reason that Drd1-SCN neurons are responsive to elevated dopaminergic tone in adulthood and account for the accelerated entrainment to a photoperiod shift observed upon specific VTA DA-neuron stimulation (Figure 6). Although increased Drd1 signaling within the developed SCN does not elicit an immediate circadian behavioral effect in constant conditions [12, 53], we hypothesize that SCN-Drd1 signaling allows the central oscillator to enter a more “entrainable” state setting the gain on entrainment cues such as light. This is supported by the evidence that: 1. Selective chemogenetic activation of Drd1-SCN neurons mimics phase responses to photic stimuli (Figure 2), 2. Drd1 expression within the SCN is necessary for a normal rate of entrainment in response to LD cycle shifts (Figures 3–5), 3. Acceleration of circadian photoentrainment after elevation of DA tone relies on the introduction of the new light phase (Figure 7). From these results, it is apparent that the incorporation of the Drd1 signaling in the SCN with the photic information is critical for appropriately timed photoentrainment. Determining how DA-dependent arousing or rewarding stimuli primes the central clock to respond more robustly to light input will be important to investigate in subsequent studies.

In summary, Drd1 mediated DA neurotransmission within the SCN is an integral component determining the rate of entrainment following changes in the prevailing light cycle. Intriguingly, arousal inducing stimuli such as introduction of a novel running wheel or exposure to sexually receptive partners, which may result in elevation of DA tone, has been shown to elicit accelerated circadian entrainment [54, 55]. Additionally, pathologies that involve aberrant DA neurotransmission such as Parkinson’s disease, depression, attention deficit hyperactivity disorder (ADHD), bipolar disorder, schizophrenia, and drug addiction are associated with abnormal circadian rhythms and sleep patterns [56–60]. Direct midbrain DA-neuron innervation to the central clock demonstrates a promising a link between dopaminergic and circadian pathologies. Delineation of the precise DA-neuronal circuitry governing circadian entrainment provides novel therapeutic targets for enhancing photoentrainment to combat symptoms of jet-lag or shift-work and alleviate the harmful effects of circadian rhythm misalignment.

STAR METHODS

CONTACT FOR REAGENT AND RESOURCE SHARING

Further information and requests should be directed to and will be fulfilled by the Lead Contact, Ali D. Güler (aguler@virginia.edu).

EXPERIMENTAL MODEL AND SUBJECT DETAILS

All animal care experiments were conducted in concordance with University of Virginia Institutional Animal Care and Use Committee (IACUC). Animals were housed in a temperature and humidity controlled vivarium (22–24°C, ~40% humidity) until experimental use on a 12-hour:12-hour light:dark cycle and were provided with food and water *ad libitum*. All experiments were conducted in mice that ranged from 2–8 months of age. In addition to wild-type C57BL6/J mice, the following mouse lines were used: *Drd1a*$^{Cre/+}$ (Drd1-Cre) [19], B6.129(Cg)-Slc6a3$^{tm1(cre)Xz}$/J (DAT-Cre) [39], B6.Cg-*Gt(ROSA)26Sor*$^{tmt(CAG-tdTomato)Hze}$/J (Ai14, ROSA26-tdTomato) [20], B6;129S-*Gt(ROSA)*$^{26Sortm34.1(CAG-Syp/tdTomato)Hze}$/J (Ai34D, ROSA26-synaptophysin-tdTomato; The Jackson Laboratory #012570). For circadian behavioral studies, littermate males were exclusively used and were backcrossed to C57BL/6 for at least 10 generations. Drd1-KO, Drd1-Cre, and wild-type littermates were raised on a special diet of Teklad 8660 (Envigo, United Kingdom) and Bio-Serv Transgenic Dough Diet (S3472, Flemington, New Jersey) until weaning to promote Drd1-KO survival, then fed with standard Teklad 8664 (Envigo, United Kingdom) on the cage floor as Drd1-KO mice were more likely to consume food when it was readily accessible [15].

METHOD DETAILS

Viral Expression and Stereotaxic Surgery—During surgery, animals were anesthetized with isoflurane (induction 5%, maintenance 2%–2.5%; Isothesia) and placed in a stereotaxic apparatus (Kopf). A heating pad was used for the duration of the surgery to maintain body temperature and ocular lubricant was applied to the eyes to prevent desiccation. A Double-floxed inverted open reading frame (DIO) cassette containing recombinant AAV were used to express specific transgenes in Cre-expressing neurons. AAV was delivered using a 10 μl syringe (Hamilton) and 26-gauge needle (Hamilton) at a flow rate of 100 nl/min driven by a microsyringe pump controller (World Precision Instruments, model Micro 4). The syringe needle was left in place for 10 minutes and was completely withdrawn 20 min after viral delivery. Following surgery, mice were administered ketoprofen (3 mg/kg) subcutaneously as an analgesic. Animals were tested at least two weeks following virus injection to ensure optimal transgene expression. Reporter expression was evaluated through immunohistochemistry. All surgical procedures were performed in sterile conditions and in accordance with University of Virginia IACUC guidelines.

Viral Constructs—Viruses were obtained from the University of North Carolina Gene Therapy Center (Chapel Hill) and the University of Pennsylvania School of Medicine Penn Vector Core. All viral cargos were cloned into the same parental construct. AAV8-hSyn-DIO-mCherry, AAV8-hSyn-DIO-hM3Dq-mCherry, AAV1-hSyn-DIO-ChR2(H134R)-eYFP, and AAV1-hSyn-DIO-Drd1-HA (500 nl; 1.1 × 10^13 viral genomes/ul) were injected into the NAc (ML: + 1.15 mm, AP: + 0.98 mm, DV: − 5.75 mm), SCN (ML: ± 0.28 mm, AP: − 0.30 mm, DV: −5.75 mm) or VTA (ML: ± 0.5 mm, AP: − 3.6 mm, DV: − 4.5 mm) depending on experimental paradigm. All coordinates are relative to bregma (George Paxinos and Keith B. J. Franklin). The original construct for AAV-DIO-Drd1-HA was developed in Larry Zweifel's lab [31].

Tracing Studies—For retrograde tracing studies, animals were injected unilaterally with 300 nl of fluorescent retrobeads (Lumafluor) directed towards the NAc or SCN. Brains were processed 3 weeks after retrobead delivery. In anterograde tracing confirmation, AAV8-hSyn-DIO-mCherry (500 nl) was delivered unilaterally into the VTA and the fiber innervation within the SCN was analyzed two weeks after surgery.

Histological Analysis and Imaging—Animals were deeply anesthetized (ketamine:xylazine, 280:80 mg/kg, i.p.) and perfused intracardially with ice cold 0.01 M phosphate buffer solution (PBS) followed by fixative solution (4% paraformaldehyde (PFA) in PBS at a pH of 7.4). After perfusion, brains were dissected and post-fixed overnight at 4°C in P FA. Brains were rinsed in PBS, transferred into 30% sucrose in PBS for 24 hours, and then frozen on dry ice. Coronal sections (30 μm) were cut with a cryostat (Microm HM 505 E). Sections were permeabilized with 0.3% Triton X-100 in PBS (PBS-T) and blocked with 3% normal donkey serum (Jackson ImmunoResearch) in PBS-T (PBS-T DS) for 30 min at room temperature. Sections were then incubated overnight in primary antibodies diluted in PBS-T DS. For visualization, sections were washed with PBS-T and incubated with appropriate secondary antibodies diluted in the blocking solution for 2 hours at room temperature. Sections were washed three times with PBS and mounted using DAPI Fluoromount-G (Southern Biotech). Images were captured on a Zeiss Axioplan 2 Imaging microscope equipped with an AxioCam MRm camera using AxioVision 4.6 software (Zeiss). The following primary antibodies were used for fluorescent labelling: anti-Drd1 (rat, 1:500, Sigma D2944), anti-TH (chicken, 1:500, Millipore AB9702; rabbit, 1:1000, Millipore AB152), anti-mCherry (rabbit, 1:1000, Abcam ab167453), anti-DsRed (rabbit, 1:1000, Clontech 632496), anti-c-Fos (rabbit, 1:5000, Calbiochem PC38; rabbit, 1:100, Santa Cruz Sc-52), anti-HA (rabbit, 1:500, Cell Signaling Technology C29F41:500). The secondary antibodies (Jackson ImmunoResearch) used were Cy2- or Cy3- conjugated donkey anti-rat IgG (1:250), donkey anti-rabbit (1:250), and goat anti-chicken (1:250).

HPLC—Fresh brains were dissected from adult wild-type male animals and 1 mm coronal slices were collected using a mouse brain matrix (Zivic Instruments). SCN samples were collected with a 1 mm in diameter tissue punch, frozen in liquid nitrogen, and stored at −80°C until further processing. Tissue punches were homogenized by sonication in 50 μl of 0.4 N perchloric acid solution. The homogenate was centrifuged at 15,000*g* for 12 min at 4°C. 25 μl of the resulting supernatant was loaded into an auto sampler connected to a high-performance liquid chromatography instrument with an electrochemical detector (Decade, Antec Leyden B.V., Zoeterwoude, The Netherlands) to measure the levels of dopamine. Retention time for DA was determined through comparison with DA standards.

Behavioral Analysis—To record the rhythm of locomotor activity, adult male mice were individually housed in activity wheel-equipped cages (Nalgene) in light-tight boxes under a 12-hour:12-hour LD cycle for at least 7 days. Fluorescent lights (100 μW/cm^2) were used for behavioral experiments. Food and water were provided *ad libitum*. Wheel running rhythms were monitored and analyzed with ClockLab collection and analysis system (Actimetrics, Wilmette, IL). The free-running period was calculated according to the onset of activity across seven days in constant darkness. Activity onset was identified through ClockLab

software as the first bin above a threshold of 5 counts preceded by at least 6 hours of inactivity and followed by at least 6 hours of activity. Offsets were determined by at least 6 hours of activity and followed by 6 hours of inactivity. When necessary, onset and offset points were edited by eye. Phase angle of entrainment was calculated as the average difference between the time of lights-off and the time of activity onset across three days during LD entrainment. All data was analyzed by a trained scorer blind to genotype or viral treatment. In constant darkness, i.p. injections were conducted under infrared light with night vision goggles.

To assess the response to a jet-lag light cycle shift, mice were entrained to an LD cycle for at least seven days, then the dark portion of the cycle was abruptly advanced or delayed six hours and locomotor activity was recorded for an additional 15 days. The days required to entrain following the shift in the light cycle was calculated. The duration of re-entrainment was defined as the number of days required to shift activity onset or offset by 6 ± 0.25 hours followed by two consecutive days of activity onset or offset within this range.

To evaluate the role of photic input during the jet-lag light cycle shift, following stable entrainment to the LD cycle for at least seven days, the dark portion of the cycle was abruptly advanced 6 hours and the mice were placed either immediately into constant darkness or after the continuation of one full LD cycle shift (Figure 4). The duration of cumulative phase shift on days 1 and 2 after the LD cycle shift was calculated relative to the onset of activity on the day prior to the shift.

To evaluate the phase responses DREADD activation or light, mice were entrained to the LD cycle for at least seven days then were placed in constant darkness for at least an additional 7 days to establish a free running period. Each animal was administered CNO (1 mg/kg in 0.9% saline) at CT 6, CT 14, or CT 22, or exposed to a 15-minute pulse of white light at either CT 14 or CT 22. Using ClockLab, a regression line was fit through activity onsets for the seven days prior to CNO or light administration and extrapolated for seven days following treatment. The duration of phase shifts was determined by measuring the time difference between the two lines on the day following the treatment.

To examine the acute effects of light on wheel running (masking), a 3-hour light pulse was delivered from ZT 14 to ZT 17. Changes in the number of wheel revolutions during application of light were quantified as percent of baseline activity at the corresponding time on the preceding day for each animal.

QUANTIFICATION AND STATISTICAL ANALYSIS

c-Fos quantification

Five 30 μm thick sections spanning through the rostro-caudal axis of the SCN and four 30 μm thick sections from the VTA were collected from each brain and labeled for c-Fos. The borders of the SCN were outlined by analysis of DAPI nuclear staining. The region of interest in μm^2 was determined using Axiovision 4.6 software and normalized to counts/ mm^2. Quantification was performed by a trained observer blind to treatment.

Statistical Analysis

Exclusion criteria for behavioral experimental animals were determined by appropriate phase angle of entrainment in LD. Mice that did not entrain to an LD cycle were excluded from analysis (n = 3 D1R-Cre mice after AAV-DIO-hM3Dq to SCN injection, 2 Drd1-Cre mice after AAV-DIO-mCherry to SCN injection, and 12 Drd1-KO mice which were used to troubleshoot the optimal titration of AAV-DIO-Drd1-HA re-expression virus). When comparing two groups of normally distributed data, Student's two tailed t-test was used. To compare the effects of genotype on days to entrain, cumulative phase shift for day 1 or day 2, and the rate of entrainment, two-way repeated-measures ANOVA was used, with *post hoc* Bonferroni's comparisons in the event of significant effects of genotype or time. All n values represent the number of mice used in each experiment. The statistical analysis is reported within the results section and figure legends. Analyses were conducted using the GraphPad Prism 6 statistical software for Windows (La Jolla California). All data are presented as mean ± standard error of the mean with $p < 0.05$ considered statistically significant.

Supplementary Material

Refer to Web version on PubMed Central for supplementary material.

Acknowledgments

We thank the members of the Deppmann, Hirsh, Condron, Siegrist, and O'Rourke labs for comments and suggestions. Additionally, we are thankful for technical assistance provided by A. Rainwater, G. Otkiran, M. Sunkara, M. Wheeler, Q. Tang and D. Holmes. Specifically, we thank J. Hirsh, E. Garren, and R. Sangston for providing the resources and assistance with HPLC. We are especially grateful for thoughtful discussion and comments on the manuscript from I. Provencio, C. Deppmann and M. Menaker. We also thank M. Carter and E. Herzog for input during the initial conceptualization of the project. This work was supported by NIH National Institute of Mental Health (NIMH) R01MH104450 (L.S.Z), NIH National Institute of General Medicinal Sciences (NIGMS) R01GM11937 (A.D.G), and UVa startup funds (A.D.G).

References

1. Moore RY, Eichler VB. Loss of a circadian adrenal corticosterone rhythm following suprachiasmatic lesions in the rat. Brain Res. 1972; 42:201–206. [PubMed: 5047187]
2. Stephan FK, Zucker I. Circadian rhythms in drinking behavior and locomotor activity of rats are eliminated by hypothalamic lesions. Proc Natl Acad Sci U S A. 1972; 69:1583–1586. [PubMed: 4556464]
3. Barion A, Zee PC. A clinical approach to circadian rhythm sleep disorders. Sleep Med. 2007; 8:566–577. [PubMed: 17395535]
4. Arble DM, Ramsey KM, Bass J, Turek FW. Circadian disruption and metabolic disease: findings from animal models. Best Pract Res Clin Endocrinol Metab. 2010; 24:785–800. [PubMed: 21112026]
5. Davidson AJ, Sellix MT, Daniel J, Yamazaki S, Menaker M, Block GD. Chronic jet-lag increases mortality in aged mice. Curr Biol. 2006; 16:R914–916. [PubMed: 17084685]
6. Provencio I, Rollag MD, Castrucci AM. Photoreceptive net in the mammalian retina. This mesh of cells may explain how some blind mice can still tell day from night. Nature. 2002; 415:493.
7. Guler AD, Ecker JL, Lall GS, Haq S, Altimus CM, Liao HW, Barnard AR, Cahill H, Badea TC, Zhao H, et al. Melanopsin cells are the principal conduits for rod-cone input to non-image-forming vision. Nature. 2008; 453:102–105. [PubMed: 18432195]
8. Altimus CM, Guler AD, Alam NM, Arman AC, Prusky GT, Sampath AP, Hattar S. Rod photoreceptors drive circadian photoentrainment across a wide range of light intensities. Nat Neurosci. 2010; 13:1107–1112. [PubMed: 20711184]

9. Hastings MH, Duffield GE, Ebling FJ, Kidd A, Maywood ES, Schurov I. Non-photic signalling in the suprachiasmatic nucleus. Biol Cell. 1997; 89:495–503. [PubMed: 9618899]
10. Golombek DA, Rosenstein RE. Physiology of circadian entrainment. Physiol Rev. 2010; 90:1063–1102. [PubMed: 20664079]
11. Mendoza J, Challet E. Circadian insights into dopamine mechanisms. Neuroscience. 2014; 282C: 230–242.
12. Weaver DR, Rivkees SA, Reppert SM. D1-dopamine receptors activate c-fos expression in the fetal suprachiasmatic nuclei. Proc Natl Acad Sci U S A. 1992; 89:9201–9204. [PubMed: 1384044]
13. Viswanathan N, Weaver DR, Reppert SM, Davis FC. Entrainment of the fetal hamster circadian pacemaker by prenatal injections of the dopamine agonist SKF 38393. J Neurosci. 1994; 14:5393–5398. [PubMed: 7916044]
14. Bender M, Drago J, Rivkees SA. D1 receptors mediate dopamine action in the fetal suprachiasmatic nuclei: studies of mice with targeted deletion of the D1 dopamine receptor gene. Brain Res Mol Brain Res. 1997; 49:271–277. [PubMed: 9387887]
15. Gallardo CM, Darvas M, Oviatt M, Chang CH, Michalik M, Huddy TF, Meyer EE, Shuster SA, Aguayo A, Hill EM, et al. Dopamine receptor 1 neurons in the dorsal striatum regulate food anticipatory circadian activity rhythms in mice. Elife. 2014; 3:e03781. [PubMed: 25217530]
16. Stephan FK, Swann JM, Sisk CL. Anticipation of 24-hr feeding schedules in rats with lesions of the suprachiasmatic nucleus. Behav Neural Biol. 1979; 25:346–363. [PubMed: 464979]
17. Stokkan KA, Yamazaki S, Tei H, Sakaki Y, Menaker M. Entrainment of the circadian clock in the liver by feeding. Science. 2001; 291:490–493. [PubMed: 11161204]
18. Rivkees SA, Lachowicz JE. Functional D1 and D5 dopamine receptors are expressed in the suprachiasmatic, supraoptic, and paraventricular nuclei of primates. Synapse. 1997; 26:1–10. [PubMed: 9097400]
19. Heusner CL, Beutler LR, Houser CR, Palmiter RD. Deletion of GAD67 in dopamine receptor-1 expressing cells causes specific motor deficits. Genesis. 2008; 46:357–367. [PubMed: 18615733]
20. Madisen L, Zwingman TA, Sunkin SM, Oh SW, Zariwala HA, Gu H, Ng LL, Palmiter RD, Hawrylycz MJ, Jones AR, et al. A robust and high-throughput Cre reporting and characterization system for the whole mouse brain. Nat Neurosci. 2010; 13:133–140. [PubMed: 20023653]
21. Welsh DK, Logothetis DE, Meister M, Reppert SM. Individual neurons dissociated from rat suprachiasmatic nucleus express independently phased circadian firing rhythms. Neuron. 1995; 14:697–706. [PubMed: 7718233]
22. Herzog ED, Takahashi JS, Block GD. Clock controls circadian period in isolated suprachiasmatic nucleus neurons. Nat Neurosci. 1998; 1:708–713. [PubMed: 10196587]
23. Antle MC, Silver R. Orchestrating time: arrangements of the brain circadian clock. Trends Neurosci. 2005; 28:145–151. [PubMed: 15749168]
24. Cao R, Robinson B, Xu H, Gkogkas C, Khoutorsky A, Alain T, Yanagiya A, Nevarko T, Liu AC, Amir S, et al. Translational control of entrainment and synchrony of the suprachiasmatic circadian clock by mTOR/4E-BP1 signaling. Neuron. 2013; 79:712–724. [PubMed: 23972597]
25. Welsh DK, Takahashi JS, Kay SA. Suprachiasmatic nucleus: cell autonomy and network properties. Annu Rev Physiol. 2010; 72:551–577. [PubMed: 20148688]
26. Armbruster BN, Li X, Pausch MH, Herlitze S, Roth BL. Evolving the lock to fit the key to create a family of G protein-coupled receptors potently activated by an inert ligand. Proc Natl Acad Sci U S A. 2007; 104:5163–5168. [PubMed: 17360345]
27. Rogan SC, Roth BL. Remote control of neuronal signaling. Pharmacol Rev. 2011; 63:291–315. [PubMed: 21415127]
28. Daan S. Tonic and phasic effects of light in the entrainment of circadian rhythms. Ann N Y Acad Sci. 1977; 290:51–59. [PubMed: 276307]
29. Takahashi JS, DeCoursey PJ, Bauman L, Menaker M. Spectral sensitivity of a novel photoreceptive system mediating entrainment of mammalian circadian rhythms. Nature. 1984; 308:186–188.
30. Missale C, Nash SR, Robinson SW, Jaber M, Caron MG. Dopamine receptors: from structure to function. Physiol Rev. 1998; 78:189–225. [PubMed: 9457173]

31. Gore BB, Zweifel LS. Genetic reconstruction of dopamine D1 receptor signaling in the nucleus accumbens facilitates natural and drug reward responses. J Neurosci. 2013; 33:8640–8649. [PubMed: 23678109]
32. Duffield GE, McNulty S, Ebling FJ. Anatomical and functional characterisation of a dopaminergic system in the suprachiasmatic nucleus of the neonatal Siberian hamster. J Comp Neurol. 1999; 408:73–96. [PubMed: 10331581]
33. Strother WN, Norman AB, Lehman MN. D1-dopamine receptor binding and tyrosine hydroxylase-immunoreactivity in the fetal and neonatal hamster suprachiasmatic nucleus. Brain Res Dev Brain Res. 1998; 106:137–144. [PubMed: 9554985]
34. Ugrumov MV, Tixier-Vidal A, Taxi J, Thibault J, Mitskevich MS. Ontogenesis of tyrosine hydroxylase-immunopositive structures in the rat hypothalamus. Fiber pathways and terminal fields. Neuroscience. 1989; 29:157–166. [PubMed: 2565561]
35. Lin LH, Pivorun EB. Analysis of serotonin, dopamine and their metabolites in the caudate putamen, the suprachiasmatic nucleus and the median raphe nucleus of euthermic and torpid deermice, Peromyscus maniculatus. Pharmacol Biochem Behav. 1989; 33:309–314. [PubMed: 2813470]
36. Nirenberg MJ, Chan J, Liu Y, Edwards RH, Pickel VM. Ultrastructural localization of the vesicular monoamine transporter-2 in midbrain dopaminergic neurons: potential sites for somatodendritic storage and release of dopamine. J Neurosci. 1996; 16:4135–4145. [PubMed: 8753875]
37. Eban-Rothschild A, Rothschild G, Giardino WJ, Jones JR, de Lecea L. VTA dopaminergic neurons regulate ethologically relevant sleep-wake behaviors. Nat Neurosci. 2016; 19:1356–1366. [PubMed: 27595385]
38. Roeper J. Dissecting the diversity of midbrain dopamine neurons. Trends Neurosci. 2013; 36:336–342. [PubMed: 23582338]
39. Zhuang X, Masson J, Gingrich JA, Rayport S, Hen R. Targeted gene expression in dopamine and serotonin neurons of the mouse brain. J Neurosci Methods. 2005; 143:27–32. [PubMed: 15763133]
40. Lammel S, Steinberg EE, Foldy C, Wall NR, Beier K, Luo L, Malenka RC. Diversity of transgenic mouse models for selective targeting of midbrain dopamine neurons. Neuron. 2015; 85:429–438. [PubMed: 25611513]
41. Blum ID, Zhu L, Moquin L, Kokoeva MV, Gratton A, Giros B, Storch KF. A highly tunable dopaminergic oscillator generates ultradian rhythms of behavioral arousal. Elife. 2014:3.
42. Kizer JS, Palkovits M, Brownstein MJ. The projections of the A8, A9 and A10 dopaminergic cell bodies: evidence for a nigral-hypothalamic-median eminence dopaminergic pathway. Brain Res. 1976; 108:363–370. [PubMed: 1276901]
43. Boulos Z, Terman M. Food availability and daily biological rhythms. Neurosci Biobehav Rev. 1980; 4:119–131. [PubMed: 6106914]
44. Krieger DT, Hauser H, Krey LC. Suprachiasmatic nuclear lesions do not abolish food-shifted circadian adrenal and temperature rhythmicity. Science. 1977; 197:398–399. [PubMed: 877566]
45. Mistlberger RE. Neurobiology of food anticipatory circadian rhythms. Physiol Behav. 2011; 104:535–545. [PubMed: 21527266]
46. Jones JR, Tackenberg MC, McMahon DG. Manipulating circadian clock neuron firing rate resets molecular circadian rhythms and behavior. Nat Neurosci. 2015; 18:373–375. [PubMed: 25643294]
47. Smyllie NJ, Chesham JE, Hamnett R, Maywood ES, Hastings MH. Temporally chimeric mice reveal flexibility of circadian period-setting in the suprachiasmatic nucleus. Proc Natl Acad Sci U S A. 2016; 113:3657–3662. [PubMed: 26966234]
48. Cahill GM, Besharse JC. Resetting the circadian clock in cultured Xenopus eyecups: regulation of retinal melatonin rhythms by light and D2 dopamine receptors. J Neurosci. 1991; 11:2959–2971. [PubMed: 1682423]
49. Doyle SE, McIvor WE, Menaker M. Circadian rhythmicity in dopamine content of mammalian retina: role of the photoreceptors. J Neurochem. 2002; 83:211–219. [PubMed: 12358745]
50. Ruan GX, Allen GC, Yamazaki S, McMahon DG. An autonomous circadian clock in the inner mouse retina regulated by dopamine and GABA. PLoS Biol. 2008; 6:e249. [PubMed: 18959477]

51. Jackson CR, Ruan GX, Aseem F, Abey J, Gamble K, Stanwood G, Palmiter RD, Iuvone PM, McMahon DG. Retinal dopamine mediates multiple dimensions of light-adapted vision. J Neurosci. 2012; 32:9359–9368. [PubMed: 22764243]

52. Nakamura T, Sato A, Kitsukawa T, Momiyama T, Yamamori T, Sasaoka T. Distinct motor impairments of dopamine D1 and D2 receptor knockout mice revealed by three types of motor behavior. Front Integr Neurosci. 2014; 8:56. [PubMed: 25076876]

53. Duffield GE, Hastings MH, Ebling FJ. Investigation into the regulation of the circadian system by dopamine and melatonin in the adult Siberian hamster (Phodopus sungorus). J Neuroendocrinol. 1998; 10:871–884. [PubMed: 9831263]

54. Yamanaka Y, Honma S, Honma K. Scheduled exposures to a novel environment with a running-wheel differentially accelerate re-entrainment of mice peripheral clocks to new light-dark cycles. Genes Cells. 2008; 13:497–507. [PubMed: 18429821]

55. Bobrzynska KJ, Mrosovsky N. Phase shifting by novelty-induced running: activity dose-response curves at different circadian times. J Comp Physiol A. 1998; 182:251–258. [PubMed: 9463922]

56. Maywood ES, O'Neill J, Wong GK, Reddy AB, Hastings MH. Circadian timing in health and disease. Prog Brain Res. 2006; 153:253–269. [PubMed: 16876580]

57. Van Veen MM, Kooij JJ, Boonstra AM, Gordijn MC, Van Someren EJ. Delayed circadian rhythm in adults with attention-deficit/hyperactivity disorder and chronic sleep-onset insomnia. Biol Psychiatry. 2010; 67:1091–1096. [PubMed: 20163790]

58. Wilson S, Argyropoulos S. Sleep in schizophrenia: time for closer attention. Br J Psychiatry. 2012; 200:273–274. [PubMed: 22474232]

59. Wulff K, Gatti S, Wettstein JG, Foster RG. Sleep and circadian rhythm disruption in psychiatric and neurodegenerative disease. Nat Rev Neurosci. 2010; 11:589–599. [PubMed: 20631712]

60. Zanini MA, Castro J, Cunha GR, Asevedo E, Pan PM, Bittencourt L, Coelho FM, Tufik S, Gadelha A, Bressan RA, et al. Abnormalities in sleep patterns in individuals at risk for psychosis and bipolar disorder. Schizophr Res. 2015

Highlights

- Absence of D1 dopamine receptor (Drd1) reduces circadian entrainment rate
- Restoration of Drd1 in the suprachiasmatic nucleus (SCN) restores entrainment rate
- Midbrain dopamine neurons innervate the SCN
- Midbrain dopamine neuron stimulation accelerates circadian entrainment

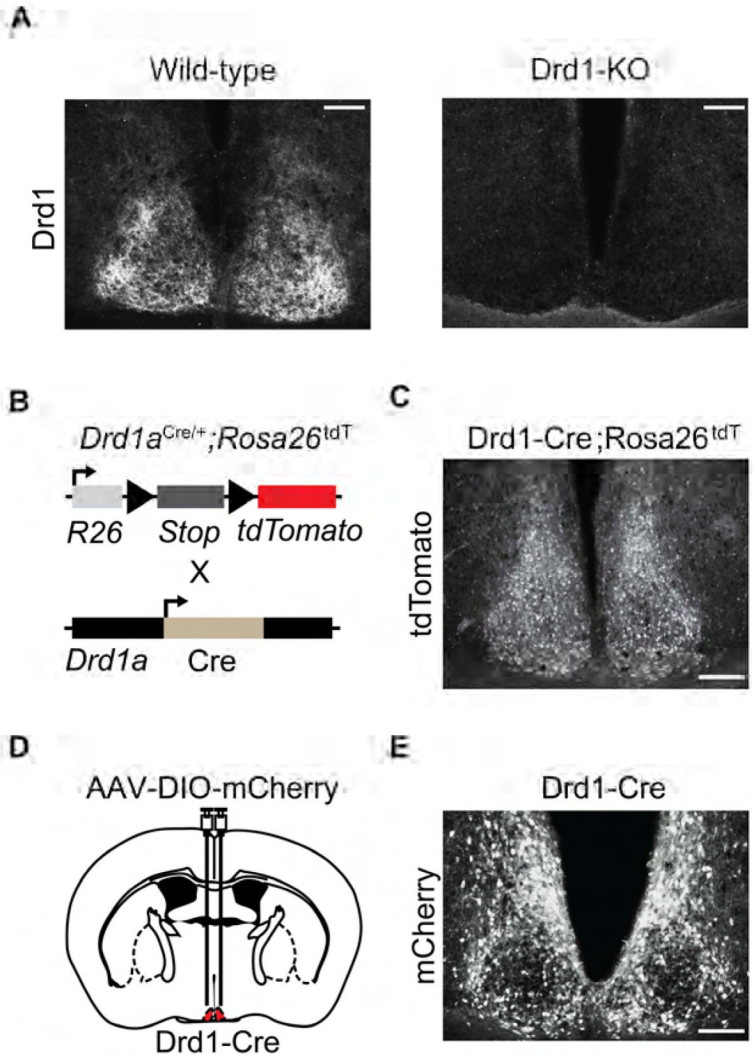

Figure 1. Drd1 is Expressed in the SCN Through Adulthood

(A) Fluorescent immunohistochemistry with Drd1 antibody labeling in the SCN of wild-type and Drd1-KO mice. Scale bar, 100 μm. (B) Schematic representation of Drd1-neuron specific Cre-mediated recombination in Drd1-Cre mice crossed with *ROSA26-tdTomato* Cre-dependent reporter mice. (C) Presence of tdTomato positive cells within the SCN (central) of *Drd1-Cre;ROSA26*^{tdT} mice. Scale bar, 100 μm. See also Figure S1. (D) Schematic diagram illustrating the site of AAV-DIO-mCherry bilateral injection to the SCN (central) of Drd1-Cre mice. (E) Fluorescent immunohistochemistry of Cre-dependent mCherry expression within the SCN of Drd1-Cre mice. See also Figure S1.

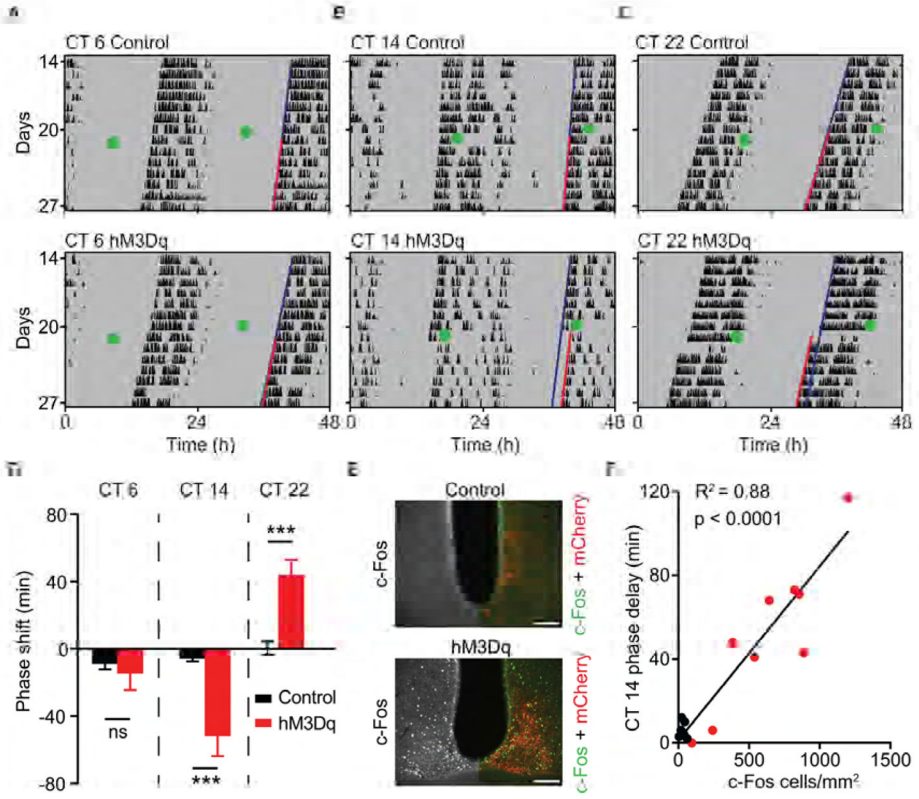

Figure 2. Phase Shift of Behavioral Rhythms by Activation of Drd1-SCN Neurons

(A) Representative double-plotted actograms (white and grey backgrounds; light and dark, respectively) of circadian time (CT) 6, (B) CT 14 and (C) CT 22 CNO-treated mCherry (control, top) and hM3Dq-mCherry (bottom) mice. Green dot indicates CNO injection (1 mg/kg, i.p.). Grey shading indicates constant darkness; dark blue line represents extended regression line derived by activity onsets prior to CNO; red line follows actual onset of activity after CNO. (D) Duration of phase shift (minutes) in response to CNO injection (1 mg/kg, i.p.), *** $p < 0.001$. (E) Fluorescent immunohistochemistry of c-Fos within the SCN (anterior) (Left hemisphere: greyscale; right hemisphere: double fluorescent immunohistochemistry of c-Fos (green) and mCherry (red) antibody labelling 120 minutes after CNO. (F) Positive correlation between the duration of phase shift and c-Fos positive cells/mm^2 within the SCN, $R^2 = 0.88$, n = 7–9/group; $p < 0.0001$, linear regression. Scale bars, 100 μm. Data are represented as mean ± SEM. See also Table S1.

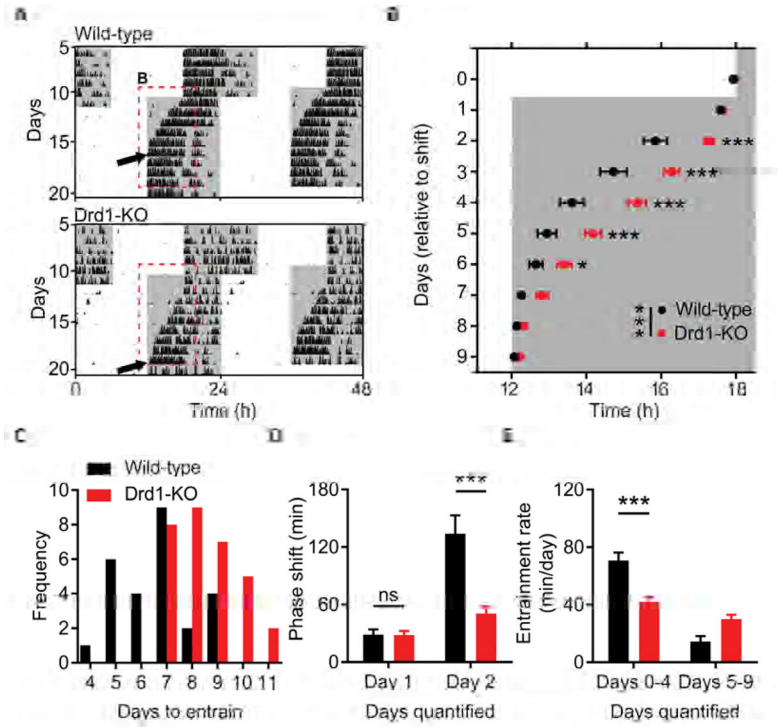

Figure 3. Delayed Entrainment of Behavioral Rhythms in Drd1-KO Mice

(A) Representative double-plotted actograms of light cycle shift comparing wild-type and Drd1-KO mice. White and grey background indicates the; light and dark phase of the LD cycle respectively. Dotted red lines outline onset data represented in b; black arrows indicate the day of entrainment. (B) Group analysis of activity onset; $F(1, 50) = 16.55$; $p = 0.0002$, repeated-measures two-way ANOVA with Bonferroni *post hoc* comparison; n = 26/group. * $p < 0.05$, ** $p < 0.01$, *** $p < 0.001$. (C) Frequency of mice per number of days required to entrain wheel running activity to the new light cycle. (D) Group analysis of day 1 and day 2 cumulative phase shift; $F(1, 50) = 11.83$; $p = 0.0012$, repeated-measures two-way ANOVA with Bonferroni *post hoc* comparison; n = 26/group. *** $p < 0.001$. (E) Rate of entrainment calculated by the slope of activity onsets divided into two segments: days 0–4 and days 5–9 relative to the light cycle shift; repeated-measures two-way ANOVA with Bonferroni *post hoc* comparison, *** $p < 0.001$. Data are represented as mean ± SEM. See also Figures S2, S3 and Table S1.

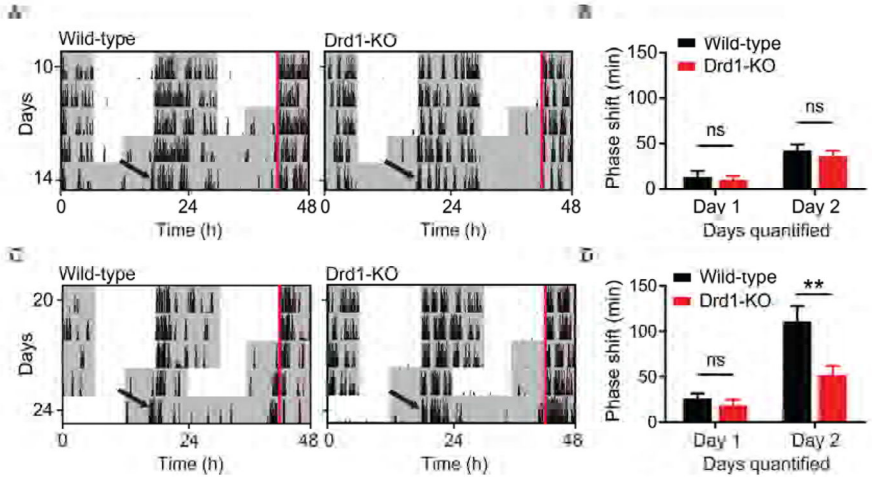

Figure 4. Drd1 Modulation of Entrainment Rate Requires Light Input

(A) Representative double-plotted actograms of wild-type and Drd1-KO mice following a 6-hour advance and immediate release into DD. (B) Group analysis of day 1 and day 2 cumulative phase shift; $F(1, 14) = 0.3684$; $p = 0.5536$, repeated-measures two-way ANOVA; n = 8/group. (C) Representative double-plotted actograms of wild-type and Drd1-KO mice following a 6-hour full LD cycle advance followed by release into DD. Red lines outline ZT 12 prior to LD shift. (D) Group analysis of day 1 and day 2 cumulative phase shift; $F(1, 14) = 7.40$; $p = 0.0166$, repeated-measures two-way ANOVA with Bonferroni *post hoc* comparison; n = 8/group. ** $p < 0.01$. Data are represented as mean ± SEM.

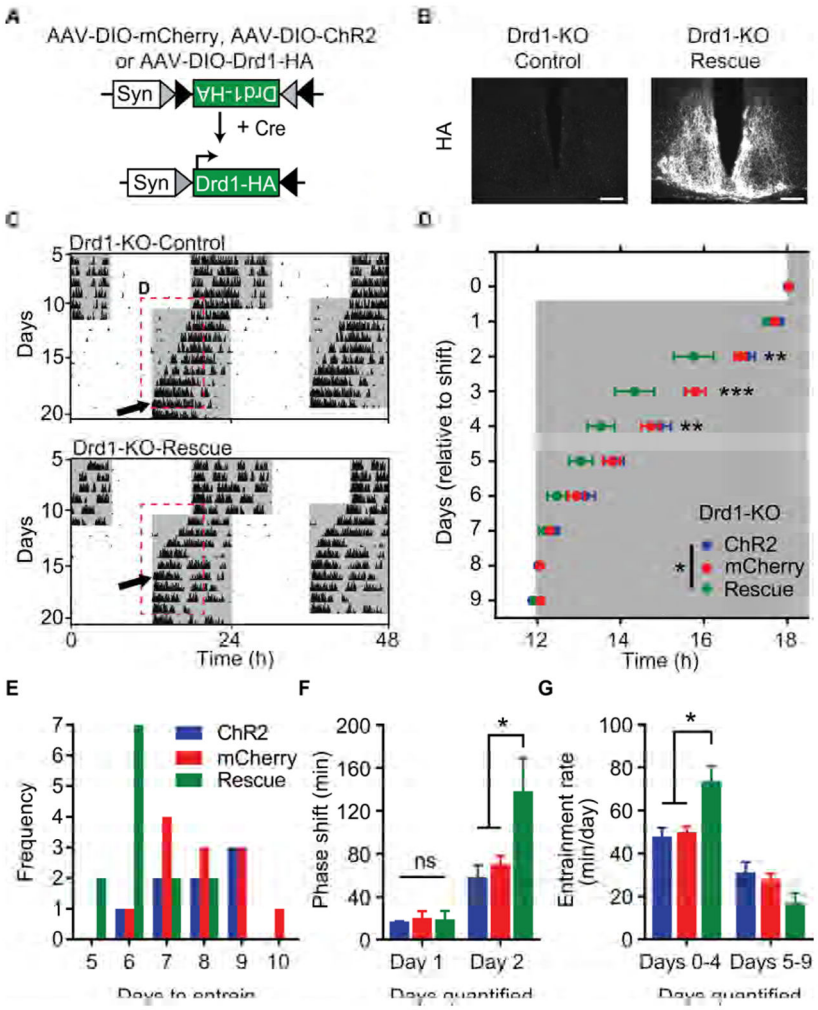

Figure 5. Viral Restoration of Drd1 within the SCN Rescues Entrainment in Drd1-KO Mice

(A) Schematic representation of the Cre-dependent AAV-DIO-Drd1-HA construct. (B) Fluorescent immunohistochemistry of HA antibody labelling within the SCN (central) of mCherry expressing controls (Drd1-KO-Control) and Drd1-HA expressing (Drd1-KO-Rescue) rescue mice. Scale bar, 100 μm. (C) Representative double-plotted actograms of light cycle shift comparing Drd1-KO-mCherry and Drd1-KO-Rescue mice. (D) Group analysis of activity onset; $F(2, 30) = 5.073$; $p = 0.0127$, repeated-measures two-way ANOVA with Bonferroni *post hoc* comparison; n = 8–13/group; * $p < 0.05$, ** $p < 0.01$, *** $p < 0.001$. (E) Frequency of mice per number of days required to entrain wheel running activity to the new light cycle. (F) Group analysis of day 1 and day 2 cumulative phase shift; $F(2, 30) = 3.319$; $p = 0.0499$, repeated-measures two-way ANOVA with Bonferroni *post hoc* comparison; * $p < 0.05$. (G) Rate of re-entrainment calculated by the slope of activity onsets, repeated-measures two-way ANOVA with Bonferroni *post hoc* comparison, ** $p < 0.01$. Data are represented as mean ± SEM. See also Figure S3 and Table S1.

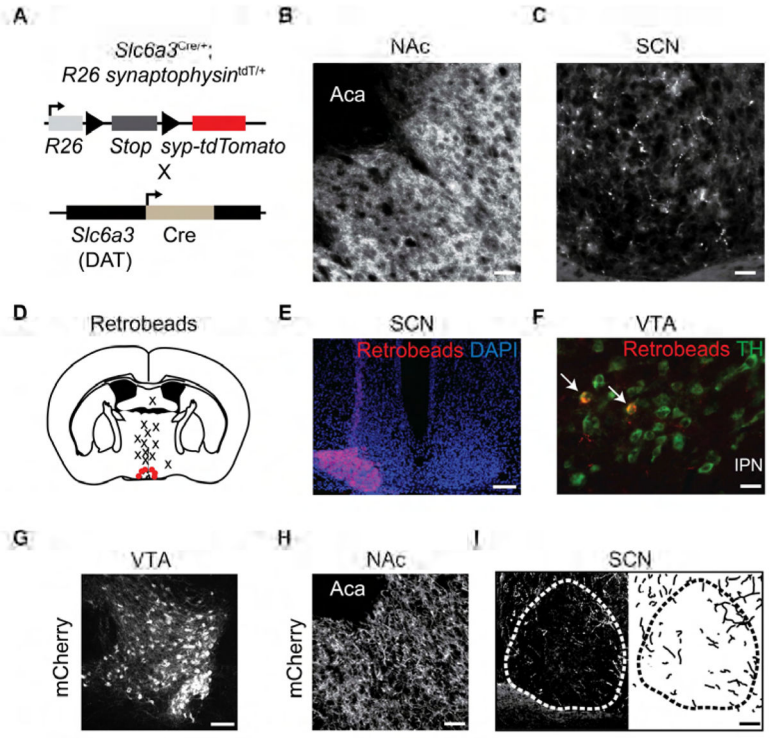

Figure 6. Identification of VTA DA-Neuron Projections and Drd1 Expression within the SCN

(A) Schematic representation of DA-neuron specific expression of synaptophysin-tdTomato in DAT-Cre mice crossed with *ROSA26-synaptophysin-tdTomato* Cre-dependent reporter mice. (B) Dense innervation within the nucleus accumbens and (C) moderate innervation within SCN (central). Scale bar, 50 μm. (D) Coronal diagram indicating retrobead target sites. Red dots specify positive SCN targeting and X's represent dorsal targeted controls. (E) Pseudo-colored images of retrobeads (beads; red) and DAPI (blue) confirming positive targeting of the SCN. Scale bar, 100 μm. (F) Fluorescent immunohistochemistry of retrobeads (red) colocalized within TH (green) positive neurons in the VTA. Scale bar, 50 μm. (G) Fluorescent immunohistochemistry with mCherry antibody labelling of VTA target site. Scale bar, 100 μm. (H) Immunoreactive mCherry fibers within the nucleus accumbens (NAc). Scale bar, 50 μm. (I) Left: Immunoreactive mCherry fibers within and around the SCN (anterior). Right: trace of innervating mCherry fibers. Scale bar, 50 μm. See also Figure S4.

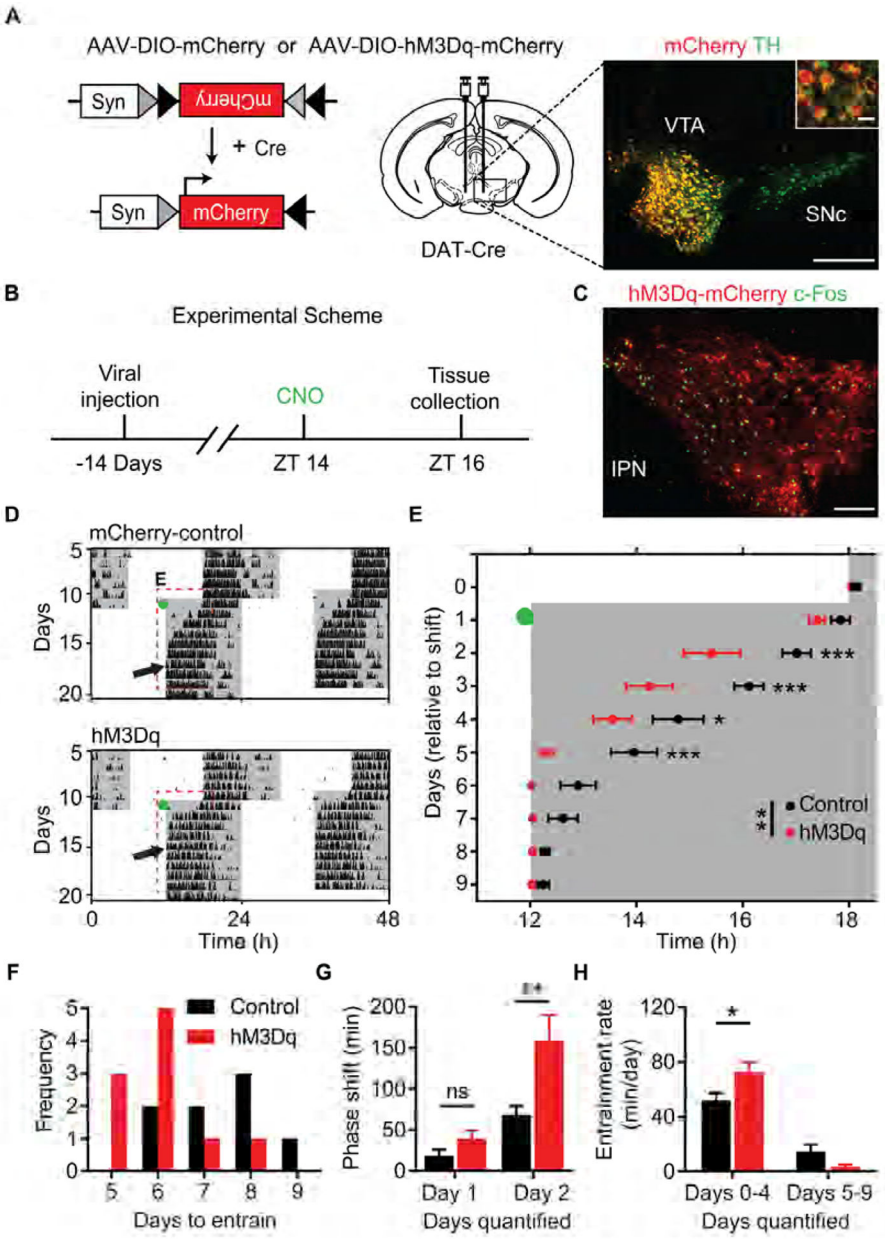

Figure 7. DREADD Activation of VTA Neurons Accelerates Circadian Entrainment

(A) Left: Design of Cre-dependent control virus, AAV-DIO-mCherry, or excitatory G_q-coupled DREADD, AAV-DIO-hM3Dq-mCherry. Syn: human synapsin promotor; Cre: Cre recombinase. Middle: Schematic illustrating injection site to the midbrain of DAT-Cre mice. Right: double fluorescent immunohistochemistry with mCherry (red) and TH (green) antibody labelling demonstrating selective transgene expression within DA-neurons of the ventral tegmental area. VTA: ventral tegmental area; SNc: Substantia nigra pars compacta. Scale bar, 200 μm; inset scale bar, 20 μm. (B) Timeline of experiment assessing CNO-induced (1mg/kg, i.p.) c-Fos expression two hours after lights-off; *Zeitgeber* time 14 (ZT 14). (C) Double fluorescent immunohistochemistry with c-Fos (green) and mCherry (red) antibody labelling reveals activation of VTA DA-neurons. Brains were collected for analysis

120 minutes after CNO injection (1mg/kg, i.p.). IPN: interpeduncular nucleus. Scale bar, 100 μm. See also Figure S1. (D) Representative double-plotted actograms of light cycle shift comparing mCherry and hM3Dq-mCherry expressing DAT-Cre mice. Green dots indicate CNO injection (1mg/kg, i.p); black arrows indicate the day of entrainment. (E) Group analysis of activity onset; $F(1, 14) = 12.74$; $p = 0.0031$, repeated-measures two-way ANOVA with Bonferroni *post hoc* comparison; n = 8–9/group; * $p < 0.05$, ** $p < 0.01$, *** $p < 0.001$. (F) Frequency of mice per number of days required to entrain wheel running activity to the new light cycle. (G) Group analysis of day 1 and day 2 cumulative phase shift; $F(1, 15) = 7.056$; $p = 0.0180$, repeated-measures two-way ANOVA with Bonferroni *post hoc* comparison; n = 8–9/group; ** $p < 0.01$. (H) Rate of entrainment calculated by the slope of activity onsets; repeated-measures two-way ANOVA with Bonferroni *post hoc* comparison; * $p < 0.05$. Data are represented as mean ± SEM. See also Figure S5 and Table S1.